metals

MDPI

Article

Aluminum-to-Steel Cladding by Explosive Welding

Gustavo H. S. F. L. Carvalho [1,*], Ivan Galvão [1,2], Ricardo Mendes [3], Rui M. Leal [1,4] and Altino Loureiro [1]

[1] Universidade de Coimbra, CEMMPRE, Departamento de Engenharia Mecânica, Rua Luís Reis Santos, 3030-788 Coimbra, Portugal; ivan.galvao@dem.uc.pt (I.G.); rui.leal@dem.uc.pt (R.M.L.); altino.loureiro@dem.uc.pt (A.L.)

[2] ISEL, Department of Mechanical Engineering, Polytechnic Institute of Lisbon, Rua Conselheiro Emídio Navarro 1, 1959-007 Lisboa, Portugal

[3] Universidade de Coimbra, ADAI/LEDAP, Departamento de Engenharia Mecânica, Rua Luís Reis Santos, 3030-788 Coimbra, Portugal; ricardo.mendes@dem.uc.pt

[4] LIDA-ESAD.CR, Polytechnic Institute of Leiria, Rua Isidoro Inácio Alves de Carvalho, 2500-321 Caldas da Rainha, Portugal

* Correspondence: gustavo.carvalho@dem.uc.pt; Tel.: +351-239-790-700

Received: 26 June 2020; Accepted: 3 August 2020; Published: 6 August 2020

Abstract: The production of aluminum-carbon steel and aluminum-stainless steel clads is challenging, and explosive welding is one of the most suitable processes to achieve them. The present work aims to investigate the coupled effect of two strategies for optimizing the production of these clads by explosive welding: the use of a low-density interlayer and the use of a low-density and low-detonation velocity explosive mixture. A broad range of techniques was used to characterize the microstructural and the mechanical properties of the welds, specifically, optical microscopy, scanning electron microscopy, energy dispersive spectroscopy, electron backscatter diffraction, microhardness and tensile-shear testing with digital image correlation analysis. Although aluminum-carbon steel and aluminum-stainless steel have different weldabilities, clads with sound microstructure and good mechanical behavior were achieved for both combinations. These results were associated with the low values of collision point and impact velocities provided by the tested explosive mixture, which made the weldability difference between these combinations less significant. The successful testing of this explosive mixture indicates that it is suitable to be used for welding very thin flyers and/or dissimilar materials that easily form intermetallic phases.

Keywords: explosive welding; interlayer; aluminum; carbon steel; stainless steel

1. Introduction

The successful production of hybrid welded structures is one of the main targets of the 21st century's industry. The development of solutions combining different materials is a great industrial challenge, which brings many technical, economic, and environmental advantages by enabling the achievement of highly efficient structures. However, manufacturing hybrid structures can be complex, especially when combining materials with significantly different physical properties. With the increase in the industrial relevance of hybrid components with unique characteristics, the complexity of welding increases and the use of conventional fusion welding technologies may not be possible. Some of the materials composing the hybrid structures tend to form very brittle intermetallic phases at high temperature, which easily results in cracking, and consequently, in a severe loss in the mechanical properties of the welded components. Thus, the solid-state welding technologies, such as the friction-based or the impact-based techniques, have a very high potential to join dissimilar materials.

The impact-based processes have the advantage of restricting the welding zone to a very narrow band at the interface of the materials and minimizing their interaction under high temperature and strain. As the impact is almost instantaneous, there is no time for heat dissipation towards the adjacent regions of the weld zone, avoiding the formation of an extensive heat affected zone and the consequent loss in mechanical properties often reported to occur in this region. In other words, the thermal cycle is short and narrow and hence causes minor microstructural changes, all very close to the welding interface. Among the impact-based technologies, the explosive welding has a prominent position since this process makes it possible to clad extensive areas, which is especially relevant for the naval, railway and automotive sectors. For these industries, aluminum and steel are widely used materials, and their welding has an especial interest by enabling the combination of the lightweight of the aluminum alloys with the low cost and the high mechanical strength of the carbon steel or with the corrosion resistance of the stainless steel.

Some research has been conducted in explosive welding of aluminum to carbon steel (Al-CS) and aluminum to stainless steel (Al-SS). Many authors have investigated the thermomechanical conditions experienced at the weld interface and their influence on the structure and on the mechanical properties of the welds [1–4]. The literature shows that these material combinations present notable differences in weldability, specifically, the range of welding parameters enabling the production of welds with good mechanical properties is wider for Al-CS welding [5]. The weldability range of the Al-SS couple is strongly conditioned by a considerable difference in the thermal conductivity of both materials [6]. However, despite the differences in Al-CS and Al-SS weldability, better welding conditions are usually achieved when the detonation and impact velocities used for joining both couples are not high [5]. High values of this parameter often lead to welds with poor mechanical properties or even to welding failure, i.e., the separation of the welded plates after the impact [7]. In dissimilar welding, this type of failure is usually associated with the formation of a thick and continuous molten layer with intermetallic composition at the interface of the welded plates [8,9].

Considering that high detonation and impact velocities may preclude or hinder the Al-CS and Al-SS welding, the optimization of the welding conditions for both combinations requires the testing of welding strategies focused on decreasing the values of these parameters. The most common strategies are the use of low-detonation velocity explosive mixtures, low explosive ratios and the use of interlayers. Among these, welding with interlayer has been the most tested. This strategy is reported to be effective for reducing the energy lost in the collision, and therefore, for preventing an extensive formation of brittle intermetallic phases. Regarding the Al-CS joining, the most reported material to be used as interlayer is commercially pure aluminum [5,10–13]. On the other hand, different materials have been tested as an interlayer in Al-SS welding, specifically, stainless steel [14,15], commercially pure aluminum [5], carbon steel [16], niobium [16], titanium [17], copper [17] and tantalum [17]. When materials from different families of both welded materials are tested as interlayers, the authors intend to explore the physical, chemical, and mechanical properties of these materials for achieving better welding conditions.

However, the use of interlayers adds a new material to the welded structure, increasing its weight and cost, especially when dense (for example, copper or carbon steel) and expensive materials (for example, niobium, tantalum, or titanium) are used with this purpose. It is already possible to weld plates with a thickness in the order of 1 mm by explosion welding. However, with the increase in design and engineering requirements, it becomes necessary to establish new strategies for welding even thinner plates. That said, it is essential to investigate not only the use of interlayers but also the development of energetic mixtures capable of providing low-detonation velocity together with lower explosive ratios. Thus, the present work is aimed to test two strategies for optimizing the production of Al-CS and Al-SS clads by explosive welding: the use of a low-density interlayer, and the development of a low-density and low-detonation velocity explosive mixture. This research analyzes the coupled effect of these two strategies on the microstructural and mechanical properties of the joints. The studied explosive mixture resulted from an intensive optimization work of the density of a previously tested explosive by controlling the volume of the sensitizer. An in-depth experimental

characterization was conducted in the welds, using a broad range of techniques, such as optical microscopy, scanning electron microscopy (SEM), energy dispersive spectroscopy (EDS), electron backscatter diffraction (EBSD), microhardness and tensile-shear testing with digital image correlation (DIC).

2. Materials and Methods

Aluminum to carbon steel and aluminum to stainless steel welded clads were produced by explosive welding in parallel full overlap joint configuration, following the set-up presented in Figure 1. All welded plates had a length of 250 mm and a width of 70 mm. The flyer was a 3 mm-thick sheet of AA6082-T6 (112 HV0.2) for both weld series, whereas a 3 mm-thick sheet of EN10130 (DC06) carbon steel (100 HV0.2) or AISI 304 stainless steel (188 HV0.2) was used as the baseplate. All the welds were produced with a 1 mm-thick interlayer of AA1050 (38 HV0.2). The explosive mixture developed to produce the welds was a low-detonation velocity emulsion-based explosive. This mixture, which is based on standard emulsion explosives [18,19], resulted from an optimization work, that was developed in the Laboratory of Energetic and Detonics (LEDAP), focused on decreasing the density of an explosive mixture through the control of the volume of the sensitizer. The weld series are identified according to the alloys of the flyer and the base plate: the Al/CS and the Al/SS series concern to aluminum to carbon steel and aluminum to stainless steel welds, respectively. All the other conditions were kept constant, i.e. the interlayer alloy, the flyer/interlayer and the interlayer/baseplate stand-off distances (STD) and the explosive thickness and ratio. Table 1 summarizes the welding conditions.

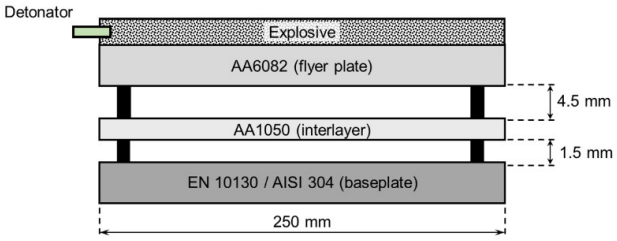

Figure 1. Schematic drawing of the welding set-up.

Table 1. Welding conditions.

Welding Conditions	Weld Series	
	Al/CS	Al/SS
Flyer plate alloy	AA6082	AA6082
Interlayer alloy	AA1050	AA1050
Baseplate alloy	EN10130	AISI 304
Flyer-interlayer STD	4.5 mm	4.5 mm
Interlayer-baseplate STD	1.5 mm	1.5 mm
Explosive Mixture	EE	EE
Explosive Mixture Density	485 kg.m^{-3}	485 kg.m^{-3}
Explosive Ratio	0.9	0.9

During welding, the detonation velocity (V_d), which has the same value as the collision point velocity (V_c) in the tested welding configuration, was measured according to Mendes et al. [20]. After the visual inspection of the welds, the samples were removed longitudinally to the welding direction and prepared for metallographic analysis according to ASTM E3-11. An optical microscope, Leica DM4000M LED (Wetzlar, Germany), was used to observe the samples, which were etched with Weck's etchant, 2% Nital and 10% oxalic acid for revealing the microstructure of the AA6082, EN10130 and AISI 304, respectively. The microstructural characterization of the welds was also conducted by SEM, using a Zeiss Merlin VP Compact microscope (Oberkochen, Germany), which was equipped with EDS. The semi-quantitative chemical composition of the welds was performed using this equipment. An accurate analysis of the grain structure of the weld interface was conducted by EBSD, using a FEI Quanta 400FEG SEM (Hillsboro, OR, USA) equipped with a TSL-EDAX EBSD

unit. The software TSL OIM Analysis 5.2 (EDAX Inc., Mahwah, NJ, USA) was used to analyze these results. The mechanical characterization of the welds was conducted by microhardness and tensile-shear testing. Microhardness profiles (HV0.2) were performed in longitudinal weld samples along the thickness direction, with a distance between indentations of 250 μm for the flyer and baseplate and 200 μm for the interlayer. Localized microhardness measurements (HV0.025) were performed at the weld interface. The microhardness tests were performed using an HMV-G Shimadzu tester (Kyoto, Japan). The tensile-shear tests were performed in quasi-static loading conditions (1 mm/min), using a 100 kN universal testing machine, Shimadzu AGS-X (Kyoto, Japan). Three specimens (removed longitudinally to the welding direction), whose design was similar to that reported by Carvalho et al. [5,16], were tested for each weld series. Figure 2 shows the geometry of the specimens, which have the original thickness of the plates. The local strain fields of the tested specimens were acquired by DIC using a GOM Aramis 5M system (Braunschweig, Germany). The procedures to prepare the specimens and to process/analyze the strain data are detailed in Leitão et al. [21]. After the tests, the fracture surface of the specimens was analyzed by SEM and the fracture mode fractions were computed by image processing.

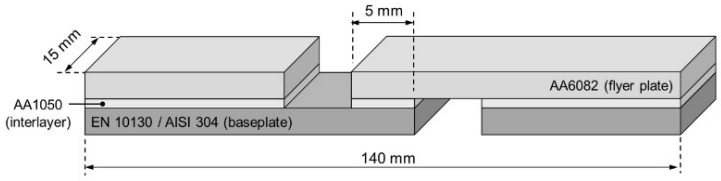

Figure 2. Details of the tensile-shear specimen.

3. Results and Discussion

3.1. Welding Results and Velocities

Table 2 shows the values measured for the detonation (V_d) and the collision point (V_c) velocities (the same values for parallel welding arrangement) and the values calculated for the impact velocity (V_p). Since the welds were produced with interlayer, two values of impact velocity were calculated: V_{pF} and V_{pFI}. V_{pF} corresponds to the velocity of the flyer plate at the instant of the first impact (the impact on the interlayer), which was computed using Gurney's equation for a one-dimensional problem in parallel configuration (Equation (1)) [22,23]. It must be noted that this equation, despite being widely accepted, presents some limitations. It ignores the acceleration of the flyer plate, and therefore, it represents only the terminal velocity [22,24]. That said, the proximity of the real value to the one calculated with Gurney's equation depends on the chosen STD.

$$V_{p_F} = \sqrt{2E}\left(\frac{3R^2}{R^2+5R+4}\right)^{\frac{1}{2}} \quad (1)$$

R is the explosive ratio (dimensionless), $\sqrt{2E}$ is the Gurney explosive's characteristic velocity (m·s^{-1}). An empirical correlation developed by Cooper [25] for ideal explosives, $\sqrt{2E} = V/2.97$, was used to estimate this parameter. The limitations of this approach were reported by Carvalho et al. [26].

V_{pFI} corresponds to the velocity of the set composed of the flyer plate and the interlayer at the instant of the second impact (the impact on the baseplate). This parameter was computed using an approximate method considering the perfectly inelastic collision theory and the momentum conservation (Equation (2)).

$$V_{p_{FI}} = \frac{m_F \cdot V_{p_F}}{m_F + m_I} \quad (2)$$

m_F is the mass of the flyer plate (kg), m_I is the mass of the interlayer (kg).

Table 2 shows that consistent welds were produced with low values of impact velocity (about 270 m·s^{-1}). In a previous study, Carvalho et al. [5] tested two explosive mixtures to produce the same type of joints: an emulsion explosive-based mixture ($V_d \approx 2800$ m·s^{-1}) and an ANFO-based mixture (V_d

≈ 2000 m·s^{-1}). Compared to that work, the present mixture made it possible to weld with much lower values of impact velocity, which resulted from its lower detonation velocity (comparing to the emulsion explosive-based mixture) and lower density (comparing to the ANFO-based mixture). In fact, although the differences in detonation velocity between the present mixture and the ANFO-based mixture are not significant, a much lower explosive ratio was possible to be used with the present mixture (0.9 vs. 2.5), decreasing the impact velocity.

Table 2. Values of detonation/collision point and impact velocities and welding results.

Weld Series	V_d, V_c (m·s^{-1})	V_{pF} (m·s^{-1})	V_{pFI} (m·s^{-1})	Welding Results
Al/CS	2055	349	262	consistent
Al/SS	2055	357	268	consistent

3.2. Interface Morphology and Microstructure

Figure 3 presents the micrographs of the longitudinal interface of the welds. Figures 3a,b show that the AA6082/AA1050 interface (flyer/interlayer interface) was similar for both weld series and was composed of well-defined typical waves. On the other hand, significant differences in morphology were observed for the dissimilar interfaces (interlayer/baseplate interface). While small curled waves were formed at the interface of the Al/CS welds (Figure 3c), a flat interface was formed for the Al/SS welds (Figure 3d). In addition to this, there is also a morphological difference related to the formation of intermediate material. For the Al/CS welds, the intermediate material was mainly formed inside the curled waves, being totally encompassed by the ductile carbon steel (Figure 3c). On the other hand, a layer of intermediate material was intermittently formed at the interface of the Al/SS welds (Figure 3d). This layer is not discernible in some zones of the weld interface, in which a direct contact between the interlayer and the baseplate material exists.

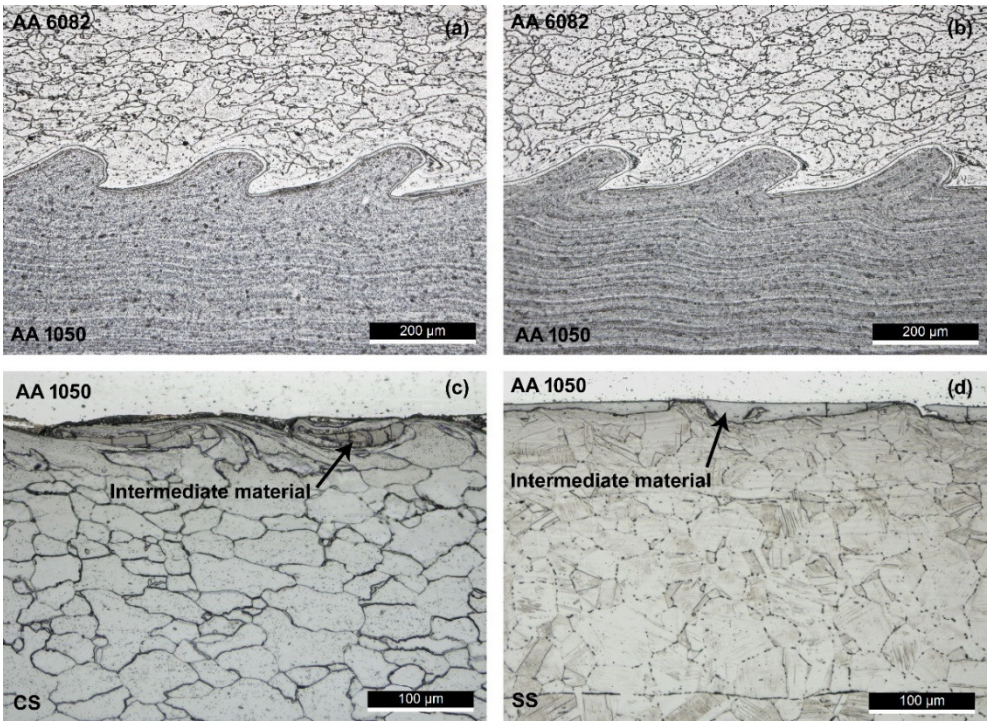

Figure 3. Micrographs of the weld interface: (**a**) Al/CS weld series—AA6082/AA1050 interface; (**b**) Al/SS weld series—AA6082/AA1050 interface; (**c**) Al/CS weld series—AA1050/CS interface; and (**d**). Al/SS weld series—AA1050/SS interface.

Comparing to the welds produced by Carvalho et al. [5], it is observed that the wave morphology of the present welds is much more similar to the morphology reported for welds

produced with the emulsion explosive-based mixture than for welds produced with the ANFO-based mixture. This makes it possible to infer that the wave morphology is deeply affected by the nature of the explosive mixture and the explosive ratio, as claimed by Mendes et al. [20] and Plaksin et al. [27] for the SS-CS welding system. On the other hand, although the ANFO-based and the present mixtures have quite similar detonation velocities, the weld interfacial waves presented significant differences in amplitude and wavelength (higher in welds produced with ANFO).

Figure 4 presents the Vickers microhardness profiles of both weld series. It shows an increase in hardness compared to the base materials hardness. This is typical from the explosive welding process and is a consequence of the strong plastic deformation promoted by the impact. Both weld series presented a general increase in hardness throughout the thickness and a slightly more pronounced increase near the interface. The AISI 304 stainless steel presented the highest increase since work hardening is an effective hardening mechanism for this type of steel.

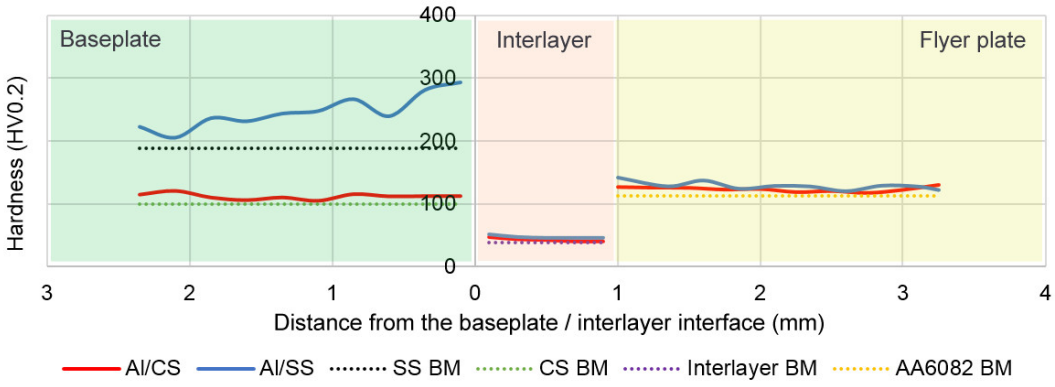

Figure 4. Microhardness (HV0.2) profiles.

Figure 5 shows the SEM micrographs of the dissimilar interface of the welds. From Figure 5a it can be observed that many cracks propagate along the intermediate material formed inside the curled waves of the Al/CS welds. The micrograph also shows that the propagation of the cracks is blocked by the wave structure, pointing to significant differences in ductility between the wave (CS) and the intermediate material. The results of the EDS analyses conducted in the regions indicated in Figure 5b (zones 1, 2 and 3) show that the intermediate material has a mixed chemical composition, being composed of Al and Fe (Table 3). The chemical composition of the intermediate region is fairly homogeneous and richer in Al. So, the formation of brittle Al-rich Fe_xAl_y intermetallic phases is expected to have occurred inside the curled waves. In good agreement with this, Carvalho et al. [7] reported the formation of Fe_4Al_{13} and Fe_2Al_5 at the interface of CS-Al explosive welds. These two intermetallic phases are the most reported in explosive welds between aluminum and steels. However, the heating and cooling conditions experienced at the interface of the explosive welds are far from equilibrium, and therefore, non-equilibrium phases may exist at the interface of the welds.

Figure 5c shows that fewer cracks propagate along the intermediate material of the Al/SS welds. The morphology of the intermediate material is also quite different for both weld series. From Figure 5d it can be observed that a much less homogenous intermediate region was formed at the interface of the Al/SS welds. Two zones are identified in this region, i.e., a lighter grey zone, which encompasses a larger area, and a darker grey zone. According to the results of the EDS analyses (Table 3), which were conducted in the regions indicated in Figure 5d, the lighter grey zone has a mixed Al-Fe chemical composition (zones 4 and 5). However, this region is richer in Al than the homogeneous intermediate material of the Al/CS welds. Besides Al and Fe, Ni and Cr, which are present in the stainless steel, were also detected. Regarding the darker grey zone, it is almost exclusively composed of Al. These results point to the formation of a heterogeneous intermediate region composed of both Al and Al-Fe intermetallic phases. Considering the chemical composition of the stainless steel, a large range of intermetallic phases may be formed at the interface of the Al/SS welds, which makes it very difficult to indicate which phases were effectively formed.

Table 3 also presents the microhardness average values measured at the intermediate regions shown in Figure 5. The microhardness values are very high compared to those of the base materials. The mixed composition, high hardness, and presence of cracks (brittleness) agree well with the formation of intermetallic phases in the intermediate regions.

Regardless of the weld series, the intermediate regions formed at the weld interface have an Al-rich intermetallic composition, which agrees well with the significant differences in the melting temperature of the Al and the two Fe alloys. In fact, since the Al has a much lower melting temperature, there is a more substantial amount of this element in the interfacial molten volumes from which the intermetallic phases are generated. Moreover, although fewer cracks are observed in the intermediate regions of the Al/SS welds, they propagate throughout the intermetallic layer, i.e., from the SS until the Al. On the other hand, the cracks in the intermediate regions of the Al/CS welds are enclosed by the curled waves, which agrees with the results reported by Carvalho et al. [5]. The ductile waves act as a protection when brittle intermetallic phases are present.

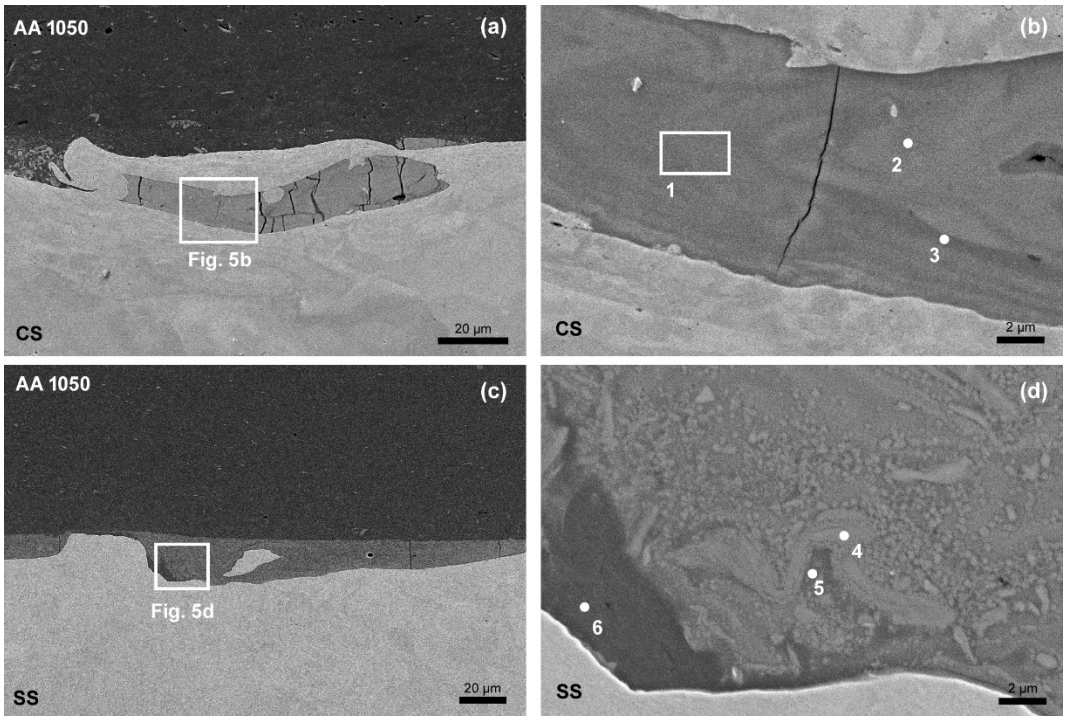

Figure 5. SEM micrographs of the dissimilar interface of the welds: (**a**), (**b**) Al/CS weld series; (**c**), (**d**) Al/SS weld series.

Table 3. Chemical composition (% at.) of the intermediate material.

Weld Series	Analysis Zone	Al	Fe	Cr	Ni	Average Microhardness (HV0.025)
Al/CS	1	67.0	33.0	--------	--------	702
	2	67.7	32.3	--------	--------	
	3	70.2	29.8	--------	--------	
Al/SS	4	82.6	13.1	3.1	1.2	414
	5	87.8	9.5	2.7	--------	
	6	97.7	2.3	--------	--------	

Figure 6 presents the results of the EBSD analysis conducted at the dissimilar interface of the welds. For the Al/CS welds, Figure 6a shows that the AA1050 and the CS have an elongated grain structure, which agrees well with the plastic deformation experienced. However, the deformation experienced by the CS composing the wave structure is especially evident. Largely deformed grains with an impressive length to width ratio are observed in this zone. In turn, a much finer and equiaxed

grain structure is observed inside the wave, pointing to the recrystallization of new grains. This region corresponds to the center of an interfacial vortex, where the most extreme strain and temperature values are usually achieved [28]. For the Al/SS welds, an elongated grain structure is also observed on the AA1050 side of the interface, as shown in Figure 6b. Regarding the SS side, this figure shows that fine equiaxed grains were formed in the nearest regions of the interface. The coupled effect of temperature and plastic deformation also promoted the recrystallization of the SS grains. Although the interaction of the welded materials is almost instantaneous in explosive welding, they experience a very strong plastic deformation and a high-temperature peak at the weld interface. The strong plastic deformation agrees with the increase in hardness next to the interface between the baseplate and the interlayer presented in Figure 4. The very high temperature and plastic deformation, as well as the occurrence of localized melting, boosted the interaction of the elements in this region, giving rise to the formation of intermetallic phases.

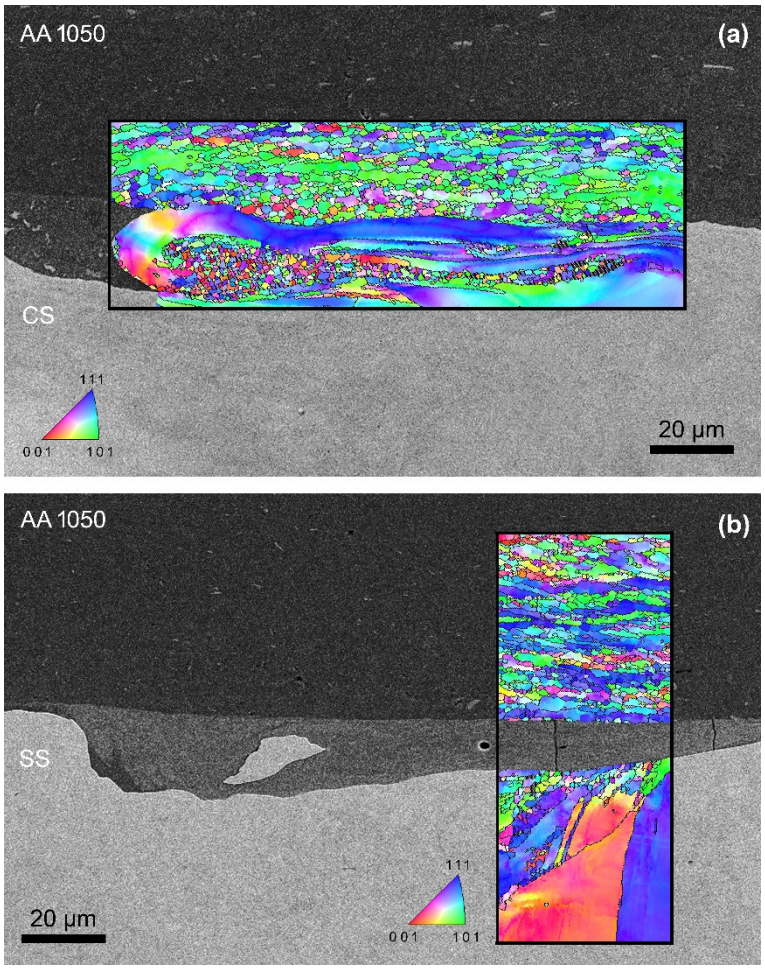

Figure 6. EBSD micrographs registered at the dissimilar interface of the welds: (**a**) Al/CS welds; (**b**) Al/SS welds.

3.3. Mechanical Properties

Table 4 displays the results of the tensile-shear tests. The table shows the maximum load value, the fracture region, and the fracture mode. For the maximum load, two values are presented for each weld series, which correspond to the lowest and the highest values obtained among all the tested specimens. Regarding the Al/CS series, it can be observed that the specimens had a very regular behavior, presenting all of them a 100% ductile fracture at the interlayer zone, with the maximum load value ranging between 4.8 kN and 5.1 kN. Figure 7a shows the Von Mises equivalent strain distribution map at the maximum load, which indicates that the strain was completely localized in

the interlayer plate. In good agreement with this, Figure 8a and Table 5 indicate that the fracture surface of the specimens consisted of shear dimples and was exclusively composed of Al, which matches the chemical composition of the AA1050 interlayer. These results indicate that the strength of the similar and dissimilar weld interfaces was higher than that of the interlayer material. The mechanical behavior of the welds was conditioned by the strength of the AA1050 and not by poor interfacial bonding.

The maximum load value of the Al/SS specimens ranged between 4.5 kN and 5.0 kN (Table 4), which was approximately the same load range observed for the Al/CS weld series. Regarding the failure region, the specimens failed in the interlayer zone, which agrees well with the Von Mises equivalent strain distribution map at the maximum load shown in Figure 7b. However, some differences were observed in the fracture mode of these specimens. The specimens with a higher maximum load presented a 100% ductile fracture through the interlayer material. Figure 8b and Table 5 show that the fracture surface of these specimens consists of shear dimples and is exclusively composed of Al. On the other hand, the specimens with a lower maximum load presented a more heterogeneous fracture surface, because they fractured both through the interlayer and at the interlayer/SS interface. While the fracture through the interlayer was ductile, with the formation of Al shear dimples (Figure 8c and Table 5), the fracture at the interlayer/SS interface was brittle. Figure 8d and Table 5 indicate that the brittle fracture surface consists of cleavage patterns and is composed of both Al and Fe. The mixed chemical composition of the fracture surface agrees well with the chemical composition of the intermediate regions formed at the dissimilar interface of these welds, which indicates that the brittle intermetallic phases partially promoted the fracture. However, despite the presence of a brittle fracture, the maximum load was not very different. This is because the percentage of brittle fracture (17%) was much lower when compared to the percentage of ductile fracture (83%).

Table 4. Maximum load in tensile-shear testing, fracture region and fracture mode.

Weld Series	Maximum Load (kN)		Fracture Region	Fracture Mode
Al/CS	Lowest	4.8	Interlayer	Ductile (100%)
	Highest	5.1	Interlayer	Ductile (100%)
Al/SS	Lowest	4.5	Interlayer[1]	Ductile (83%) and Brittle (17%)
	Highest	5.0	Interlayer	Ductile (100%)

[1] The fracture occurred through the interlayer and through the interlayer/SS interface.

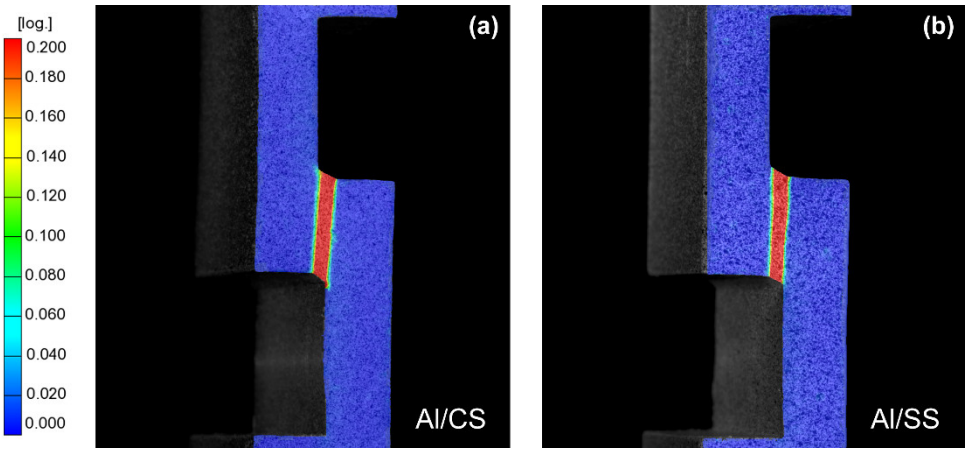

Figure 7. Von Mises equivalent strain distribution map: (**a**) Al/CS weld—ductile fracture; (**b**) Al/SS weld—ductile fracture.

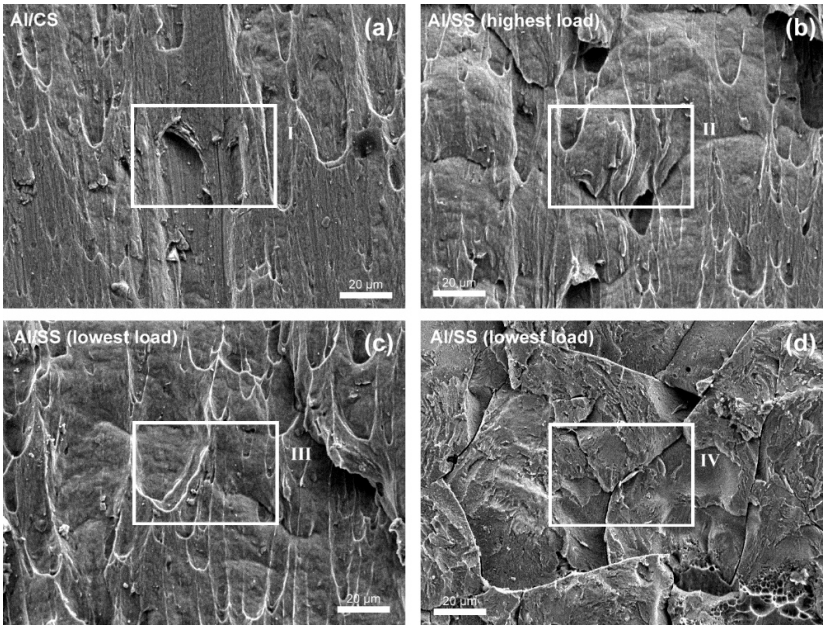

Figure 8. SEM micrographs of the fracture surface of the welds: (**a**) Al/CS welds; (**b**) Al/SS welds—highest maximum load; (**c**,**d**) Al/SS welds—lowest maximum load.

Table 5. Chemical composition (% at.) of the fracture surface of the welds.

Analysis Zone	Al	Fe	Cr	Ni	Si
I	100	--------	--------	--------	--------
II	99.8	--------	--------	--------	0.2
III	100	--------	--------	--------	--------
IV	78.2	12.9	3.6	3.2	2.1

The differences between Al/CS and Al/SS welds in the tensile-shear tests occur mainly because of two reasons: the intermetallic formation and the interfacial microstructure. These differences lie mainly in the appearance of a brittle fracture percentage. The intermetallic formation of the Al/SS is more complex because of the presence of more alloying elements (Cr and Ni) that can form intermetallic phases with Al, Fe and complex phases combining more than these two elements. The interfacial microstructure also represents a critical factor on mechanical performance. The curled wavy interface of the Al/CS improved the mechanical performance, once the brittle intermetallic phases formed during the process were surrounded by ductile material (the waves). In other words, it avoids the intermetallic phases from being propitious regions to an uninterrupted propagation of a brittle fracture. Carvalho et al. [5] detailed this beneficial effect of the curled wave compared to flat interfaces.

The interfacial microstructure has a major role in explosive welding. The presence of waves (typical or curled wave) often leads to a better mechanical performance of the joint. Some recent works make it possible to better understand and predict the weld interface. While Carvalho et al. [26] study the prediction of a wavy interface in general, Carvalho et al. [16] study the prediction of curled waves specifically. These studies support the fact that the interfacial microstructure of the Al/CS welds significantly contributed to the best mechanical performance.

In a previous work [5], the Al-CS and Al-SS pairs were welded with a slightly lower collision point velocity and higher explosive ratio than the present work. The collision point velocity was not significantly different, but the higher explosive ratio led to higher impact velocity values. This means that the impact pressure was also more intense, which led to more substantial plastic deformation and strain hardening. It is important to note that two aspects should be balanced for the selection of the most suitable impact velocity in dissimilar welding of materials with easy formation of brittle

intermetallic phases, specifically, the volume of intermetallic phases formed and the plastic deformation experienced by the materials at the interface. Until a threshold in impact velocity, higher values provide welds with better mechanical behavior by increasing the interfacial plastic deformation. After reaching this threshold, the increase in impact velocity only leads to the increase in the volume of brittle phases at the interface, and consequently, to the weakening of the welds. However, this threshold strongly depends on the microstructure of the weld interface, since, when curled waves are formed, the interface presents a higher ability to accommodate the volume of brittle phases generated during welding.

When higher collision point velocities were used on the same previous work [5], the results were rather irregular, considering that some welds failed during specimens preparation due to the poor bonding strength. The present work is between the two situations, offering an alternative of parameters that can be used especially in cases of flyers with lower thickness and density, in which mixtures of low velocity and high ratio, as used in previous works [5], may not be suitable. It is a significant advance for the welding of very thin plates of low-density materials, such as the aluminum alloys.

3.4. Energetic Mixture Analysis

In explosive welding, the challenge of the process is not only to define suitable welding parameters. After defining the best parameters, it is necessary to find energetic materials that can provide the parameters needed, such as detonation and impact velocities. One of the usual problems is that there are not too many energetic materials with adequate parameters, especially when low detonation velocities are preferred. In order to detonate, many of the low-detonation velocity explosive mixtures need a higher thickness of material than the high-detonation velocity mixtures. This fact leads to an issue, i.e., despite a lower detonation velocity, once the thickness of explosive mixture is high, the explosive ratio will be higher, and consequently, the impact velocity will increase too. In other words, choosing a low-detonation velocity explosive does not mean that the energy of the collision will be significantly lower due to the increase in the explosive ratio [5,6,9,20].

One of the topics of the present work is the study of a novel explosive mixture that has a low detonation velocity, low density and that does not need a high thickness to detonate, i.e. it can be used with a low explosive ratio. Figure 9 shows a sample of results from different works relating the detonation velocity with the explosive ratio used. The figure illustrates the abovementioned fact that, except for the mixture used in the present research, the explosive mixtures of lower detonation velocities tend to be used with higher explosive ratios. Since low-detonation velocity explosives usually need higher thickness, most explosive mixtures depart from the graph's origin. This proves the importance of developing mixtures that provide low detonation velocities and can detonate with thin layers. As referred above, the mixture developed in LEDAP and used in the present research has low detonation velocity, low density and does not need a high thickness to detonate. This is an important issue, especially for the welding of low-thickness and low-density flyers.

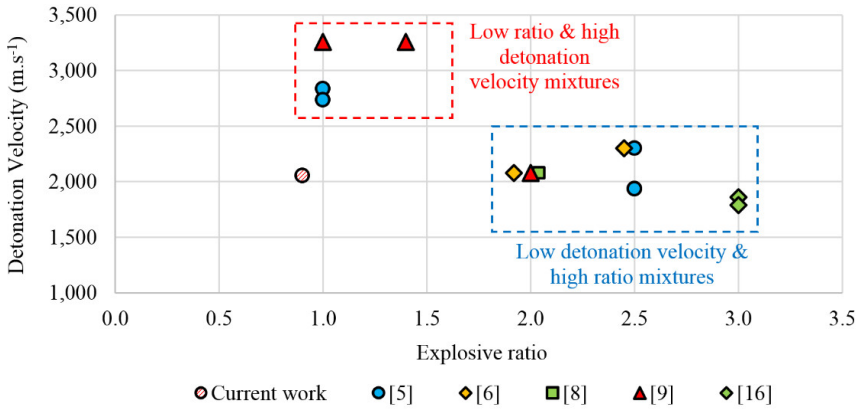

Figure 9. Graph relating the detonation velocity and the explosive ratio of tested explosive mixtures.

Deepening the analysis beyond the low detonation velocity and ratio, the density of the energetic material deserves attention due to its influence on the ratio. The achievement of low ratio explosive welds is facilitated by the use of low-density explosive mixtures. That said, an important novelty of the present research is the achievement of sound welds and proper detonation using a very low-density energetic mixture. Figure 10 compares 58 works from the literature relating the density (ρ_{exp}) and the detonation velocity (V_d) of explosive mixtures used for planar explosive welding. A point with multiple references indicates that all the references listed for that point have the same values of density and detonation velocity and are therefore located in the same position on the graph. For works in which the detonation velocity of a specific mixture was informed as a range (instead of a single measured value); in order to represent any possibility of detonation velocity within the range, two points concerning its maximum and minimum values were plotted. The figure shows that the mixture developed in the present work belongs to a small group of mixtures located closer to the origin of the graph. It should be noted that the detonation velocity of an explosive mixture may vary according to other properties beyond the density, such as the thickness of the mixture [15]. However, the data on the properties of the tested explosive mixtures are very limited in the literature.

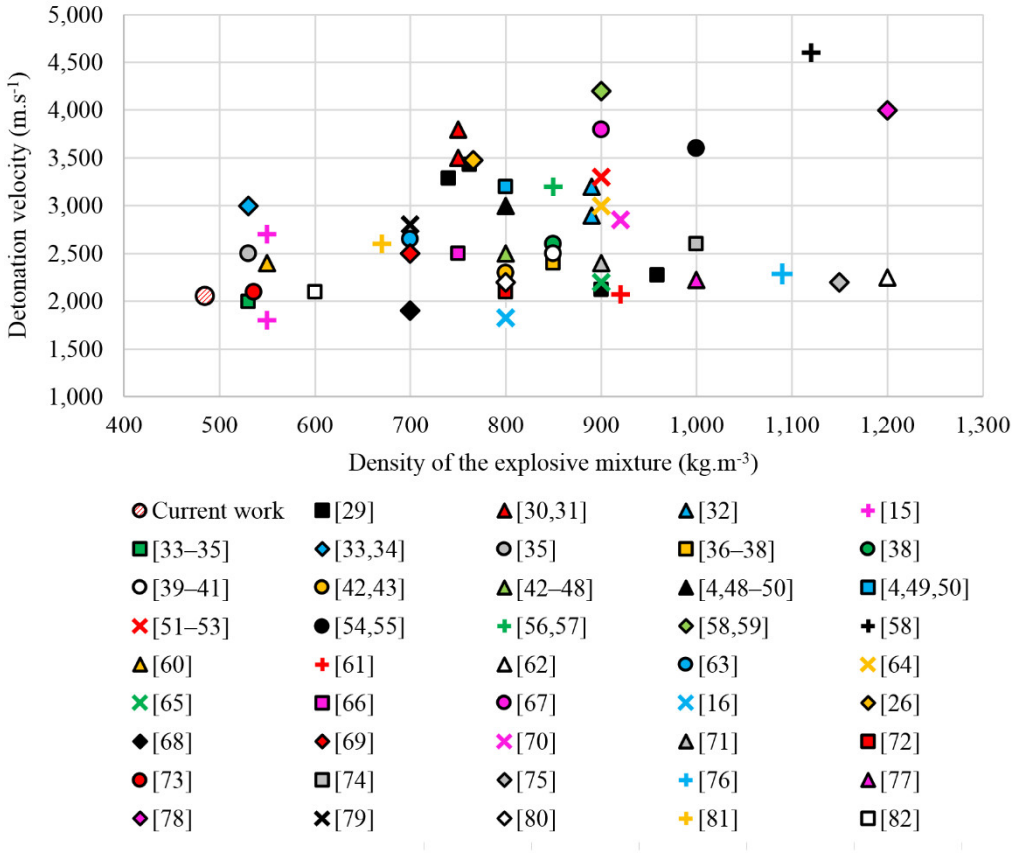

Figure 10. Graph relating the detonation velocity and the density of tested explosive mixtures. Data from [4,15,16,26,29–82].

In order to examine the detonation velocity and the density together, they were multiplied by one another. In this way, the two parameters were ordered on a single axis and are shown in Figure 11. The mixture tested in the present work presents one of the lowest values of $V_d.\rho_{exp}$ among all the 58 works analyzed. Figures 9–11 show that the mixture is outside the groups of mixtures most tested in explosive welding literature. One of the limitations of the explosive welding process is precisely the difficulty of welding very thin plates (mainly the flyer plate). It happens due to the complexity of detonating thin layers of energetic mixtures that can provide the parameters needed, and because of the damage that the detonation causes on thin plates. This new mixture of energetic material enables the possibility of a mixture with low-density capable of providing low-detonation velocity, low

explosive ratio and low-impact velocity. This is particularly important because it facilitates the welding of thinner materials. Beyond this fact, the tested mixture also has the advantage of reducing the energy conditions at the weld interface, which is significant for material combinations that tend to form intermetallic phases. On the one hand, if these combinations do not form favorable interface morphologies, such as curled waves, the large intermetallic volumes are very detrimental to the mechanical properties of the welds. On the other hand, even when favorable interfaces are formed, it is already established that large volumes of intermetallic phases may affect the physical phenomena at the weld interface, specifically, the solidification time of the interfacial molten material, conditioning the bonding conditions [7].

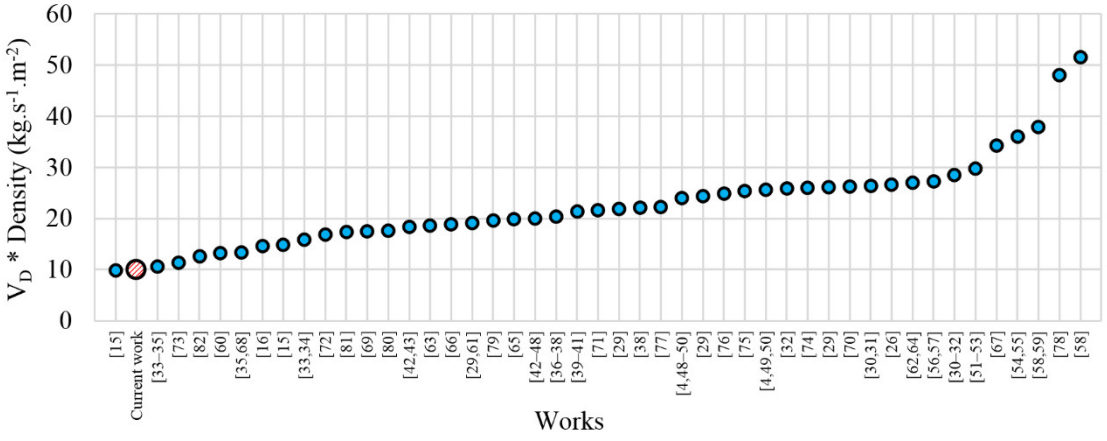

Figure 11. Graph relating on a single axis the detonation velocity and the density of the explosive mixture.

4. Conclusions

The present work has investigated the coupled effect of two strategies for optimizing the production of aluminum-carbon steel and aluminum-stainless steel clads by explosive welding: the use of a low-density interlayer, and the development of a low-density and low-detonation velocity explosive mixture. The following conclusions can be drawn:

- The coupled use of an interlayer and a low-density and low-detonation velocity explosive mixture is an effective strategy for producing aluminum-to-carbon steel and aluminum-to-stainless steel clads with sound microstructure and good mechanical behavior;
- The difference in weldability of aluminum-carbon steel and aluminum-stainless steel couples are less significant when welding under low energetic conditions;
- The tested low-density explosive mixture detonated with low detonation velocity, using a low explosive ratio, which resulted in welding with low values of both collision point velocity and impact velocity;
- Given to its properties of low-detonation velocity, low-density and the ability to detonate in small explosive thickness, the tested mixture is suitable to be used for welding very thin flyers and for welding dissimilar materials that tend to form intermetallic phases.

Author Contributions: Conceptualization, G.H.S.F.L.C. and I.G.; methodology, G.H.S.F.L.C., I.G. and R.M.L.; investigation, G.H.S.F.L.C., I.G. and R.M.L.; resources, R.M. and A.L.; writing—original draft preparation and edition, G.H.S.F.L.C. and I.G.; writing—review, R.M.L., R.M. and A.L.; supervision, R.M. and A.L.; project administration, A.L.; funding acquisition, A.L. All authors have read and agreed to the published version of the manuscript.

Funding: This research was funded by FEDER and FCT, as indicated in the acknowledgements.

Acknowledgments: This research is sponsored by FEDER funds through the program COMPETE—Programa Operacional Factores de Competitividade—and by national funds through FCT—Fundação para a Ciência e a Tecnologia, under the project UIDB/00285/2020.

Conflicts of Interest: The authors declare no conflict of interest.

References

1. Li, Y.; Hashimoto, H.; Sukedai, E.; Zhang, Y.; Zhang, Z. Morphology and structure of various phases at the bonding interface of Al/steel formed by explosive welding. *J. Electron Microsc.* **2000**, *49*, 5–16, doi:10.1093/oxfordjournals.jmicro.a023791.
2. Li, X.; Ma, H.; Shen, Z. Research on explosive welding of aluminum alloy to steel with dovetail grooves. *Mater. Des.* **2015**, *87*, 815–824, doi:10.1016/j.matdes.2015.08.085.
3. Guo, X.; Fan, M.; Wang, L.; Ma, F. Bonding Interface and Bending Deformation of Al/316LSS Clad Metal Prepared by Explosive Welding. *J. Mater. Eng. Perform.* **2016**, *25*, 2157–2163, doi:10.1007/s11665-016-2057-9.
4. Kaya, Y. Microstructural, Mechanical and Corrosion Investigations of Ship Steel-Aluminum Bimetal Composites Produced by Explosive Welding. *Metals* **2018**, *8*, 544, doi:10.3390/met8070544.
5. Carvalho, G.H.S.F.L.; Galvão, I.; Mendes, R.; Leal, R.M.; Loureiro, A. Microstructure and mechanical behaviour of aluminium-carbon steel and aluminium-stainless steel clads produced with an aluminium interlayer. *Mater. Charact.* **2019**, *155*, 109819, doi:10.1016/j.matchar.2019.109819.
6. Carvalho, G.H.S.F.L.; Galvão, I.; Mendes, R.; Leal, R.M.; Loureiro, A. Explosive welding of aluminium to stainless steel. *J. Mater. Process. Technol.* **2018**, *262*, 340–349, doi:10.1016/j.jmatprotec.2018.06.042.
7. Carvalho, G.H.S.F.L.; Galvão, I.; Mendes, R.; Leal, R.M.; Loureiro, A. Formation of intermetallic structures at the interface of steel-to-aluminium explosive welds. *Mater. Charact.* **2018**, *142*, 432–442, doi:10.1016/j.matchar.2018.06.005.
8. Carvalho, G.H.S.F.L.; Galvão, I.; Mendes, R.; Leal, R.M.; Loureiro, A. Influence of base material properties on copper and aluminium–copper explosive welds. *Sci. Technol. Weld. Join.* **2018**, *23*, 501–507, doi:10.1080/13621718.2017.1417783.
9. Carvalho, G.H.S.F.L.; Galvão, I.; Mendes, R.; Leal, R.M.; Loureiro, A. Weldability of aluminium-copper in explosive welding. *Int. J. Adv. Manuf. Technol.* **2019**, *103*, 3211–3221, doi:10.1007/s00170-019-03841-9.
10. Han, J.H.; Ahn, J.P.; Shin, M.C. Effect of interlayer thickness on shear deformation behavior of AA5083 aluminum alloy/SS41 steel plates manufactured by explosive welding. *J. Mater. Sci.* **2003**, *38*, 13–18, doi:10.1023/A:1021197328946.
11. Tricarico, L.; Spina, R.; Sorgente, D.; Brandizzi, M. Effects of heat treatments on mechanical properties of Fe/Al explosion-welded structural transition joints. *Mater. Des.* **2009**, *30*, 2693–2700, doi:10.1016/j.matdes.2008.10.010.
12. Costanza, G.; Crupi, V.; Guglielmino, E.; Sill, A.; Tata, M.E. Metallurgical characterization of an explosion welded aluminum/steel joint. *Metall. Ital.* **2016**, *108*, 17–22.
13. Corigliano, P.; Crupi, V.; Guglielmino, E.; Mariano Sili, A. Full-field analysis of AL/FE explosive welded joints for shipbuilding applications. *Mar. Struct.* **2018**, *57*, 207–218, doi:10.1016/j.marstruc.2017.10.004.
14. Izuma, T.; Hokamoto, K.; Fujita, M.; Aoyagi, M. Single-shot explosive welding of hard-to-weld A5083/SUS304 clad using SUS304 intermediate plate. *Weld. Int.* **1992**, *6*, 941–946, doi:10.1080/09507119209548320.
15. Hokamoto, K.; Izuma, T.; Fujita, M. New explosive welding technique to weld aluminum alloy and stainless steel plates using a stainless steel intermediate plate. *Metall. Trans. A* **1993**, *24*, 2289–2297, doi:10.1007/BF02648602.
16. Carvalho, G.H.S.F.L.; Galvão, I.; Mendes, R.; Leal, R.M.; Loureiro, A. Explosive welding of aluminium to stainless steel using carbon steel and niobium interlayers. *J. Mater. Process. Technol.* **2020**, *283*, 116707, doi:10.1016/j.jmatprotec.2020.116707.
17. Aceves, S.M.; Espinosa-Loza, F.; Elmer, J.W.; Huber, R. Comparison of Cu, Ti and Ta interlayer explosively fabricated aluminum to stainless steel transition joints for cryogenic pressurized hydrogen storage. *Int. J. Hydrogen Energy* **2015**, *40*, 1490–1503, doi:10.1016/j.ijhydene.2014.11.038.
18. Mendes, R.; Ribeiro, J.; Plaksin, I.; Campos, J.; Tavares, B. Differences between the detonation behavior of emulsion explosives sensitized with glass or with polymeric micro-balloons. *J. Phys. Conf. Ser.* **2014**, *500*, 1–6, doi:10.1088/1742-6596/500/5/052030.

19. Mendes, R.; Ribeiro, J.B.; Plaksin, I.; Campos, J. Non Ideal Detonation of Emulsion Explosives Mixed with Metal Particles. *AIP Conf. Proc.* **2012**, *1426*, 267–270, doi:10.1063/1.3686270.
20. Mendes, R.; Ribeiro, J.B.; Loureiro, A. Effect of explosive characteristics on the explosive welding of stainless steel to carbon steel in cylindrical configuration. *Mater. Des.* **2013**, *51*, 182–192, doi:10.1016/j.matdes.2013.03.069.
21. Leitão, C.; Galvão, I.; Leal, R.M.; Rodrigues, D.M. Determination of local constitutive properties of aluminium friction stir welds using digital image correlation. *Mater. Des.* **2012**, *33*, 69–74, doi:10.1016/j.matdes.2011.07.009.
22. Kennedy, J.E. *Gurney Energy of Explosives: Estimation of the Velocity and Impulse Imparted to Driven Metal*; Sandia Laboratories: Albuquerque, NM, USA, 1970; ISBN SC-RR-70-790.
23. El-Sobky, H. Mechanics of Explosive Welding. In *Explosive Welding, Forming and Compaction*, Blazynski, T.Z., Ed.; Springer: Dordrecht, The Netherlands, 1983; pp. 189–217.
24. Patterson, R.A. Fundamentals of Explosion Welding. In *ASM Handbook—Volume 6: Welding, Brazing and Soldering*; ASM International: Materials Park, OH, USA, 1993; pp. 160–164.
25. Cooper, P.W. *Explosive Engineering*; Wiley-VCH: New York, NY, USA, 1996; ISBN 0-471-18636-8.
26. Carvalho, G.H.S.F.L.; Mendes, R.; Leal, R.M.; Galvão, I.; Loureiro, A. Effect of the flyer material on the interface phenomena in aluminium and copper explosive welds. *Mater. Des.* **2017**, *122*, 172–183, doi:10.1016/j.matdes.2017.02.087.
27. Plaksin, I.; Campos, J.; Ribeiro, J.; Mendes, R.; Direito, J.; Braga, D.; Pruemmer, R. Novelties in physics of explosive welding and powder compaction. *J. Phys. IV* **2003**, *110*, 797–802, doi:10.1051/jp4:20020791.
28. Bataev, I.A.; Bataev, A.A.; Mali, V.I.; Bataev, V.A.; Balaganskii, I.A. Structural Changes of Surface Layers of Steel Plates in the Process of Explosive Welding. *Met. Sci. Heat Treat.* **2014**, *55*, 509–513, doi:10.1007/s11041-014-9663-7.
29. Loureiro, A.; Mendes, R.; Ribeiro, J.B.; Leal, R.M.; Galvão, I. Effect of explosive mixture on quality of explosive welds of copper to aluminium. *Mater. Des.* **2016**, *95*, 256–267, doi:10.1016/j.matdes.2016.01.116.
30. Durgutlu, A.; Gülenç, B.; Findik, F. Examination of copper/stainless steel joints formed by explosive welding. *Mater. Des.* **2005**, *26*, 497–507, doi:10.1016/j.matdes.2004.07.021.
31. Kahraman, N.; Gülenç, B.; Findik, F. Joining of titanium/stainless steel by explosive welding and effect on interface. *J. Mater. Process. Technol.* **2005**, *169*, 127–133, doi:10.1016/j.jmatprotec.2005.06.045.
32. Zhao, H.; Li, P.; Zhou, Y.; Huang, Z.; Wang, H. Study on the Technology of Explosive Welding Incoloy800-SS304. *J. Mater. Eng. Perform.* **2011**, *20*, 911–917, doi:10.1007/s11665-010-9712-3.
33. Manikandan, P.; Hokamoto, K.; Raghukandan, K.; Chiba, A.; Deribas, A.A. The effect of experimental parameters on the explosive welding of Ti and stainless steel. *Sci. Technol. Energ. Mater.* **2005**, *66*, 370–374.
34. Manikandan, P.; Hokamoto, K.; Fujita, M.; Raghukandan, K.; Tomoshige, R. Control of energetic conditions by employing interlayer of different thickness for explosive welding of titanium/304 stainless steel. *J. Mater. Process. Technol.* **2008**, *195*, 232–240, doi:10.1016/j.jmatprotec.2007.05.002.
35. Inao, D.; Mori, A.; Tanaka, S.; Hokamoto, K. Explosive Welding of Thin Aluminum Plate onto Magnesium Alloy Plate Using a Gelatin Layer as a Pressure-Transmitting Medium. *Metals* **2020**, *10*, 106, doi:10.3390/met10010106.
36. Mousavi, S.A.A.A.; Sartangi, P.F. Effect of post-weld heat treatment on the interface microstructure of explosively welded titanium–stainless steel composite. *Mater. Sci. Eng. A* **2008**, *494*, 329–336, doi:10.1016/j.msea.2008.04.032.
37. Mousavi, S.A.A.A.; Sartangi, P.F. Experimental investigation of explosive welding of cp-titanium/AISI 304 stainless steel. *Mater. Des.* **2009**, *30*, 459–468, doi:10.1016/j.matdes.2008.06.016.
38. Duan, M.; Wang, Y.; Ran, H.; Ma, R.; Wei, L. Study on Inconel 625 Hollow Structure Manufactured by Explosive Welding. *Mater. Manuf. Process.* **2014**, *29*, 1011–1016, doi:10.1080/10426914.2014.921707.
39. Zhang, H.; Jiao, K.X.; Zhang, J.L.; Liu, J. Experimental and numerical investigations of interface characteristics of copper/steel composite prepared by explosive welding. *Mater. Des.* **2018**, *154*, 140–152, doi:10.1016/j.matdes.2018.05.027.
40. Zhang, H.; Jiao, K.X.; Zhang, J.L.; Liu, J. Microstructure and mechanical properties investigations of copper-steel composite fabricated by explosive welding. *Mater. Sci. Eng. A* **2018**, *731*, 278–287, doi:10.1016/j.msea.2018.06.051.
41. Yang, M.; Ma, H.; Shen, Z. Study on explosive welding of Ta2 titanium to Q235 steel using colloid water as a covering for explosives. *J. Mater. Res. Technol.* **2019**, *8*, 5572–5580, doi:10.1016/j.jmrt.2019.09.025.

42. Ma, R.; Wang, Y.; Wu, J.; Duan, M. Explosive welding method for manufacturing ITER-grade 316L(N)/CuCrZr hollow structural member. *Fusion Eng. Des.* **2014**, *89*, 3117–3124, doi:10.1016/j.fusengdes.2014.10.001.
43. Ma, R.; Wang, Y.; Wu, J.; Duan, M. Investigation of microstructure and mechanical properties of explosively welded ITER-grade 316L(N)/CuCrZr hollow structural member. *Fusion Eng. Des.* **2015**, *93*, 43–50, doi:10.1016/j.fusengdes.2015.02.018.
44. Liu, Y.; Li, C.; Hu, X.; Yin, C.; Liu, T. Explosive Welding of Copper to High Nitrogen Austenitic Stainless Steel. *Metals* **2019**, *9*, 339, doi:10.3390/met9030339.
45. Honarpisheh, M.; Asemabadi, M.; Sedighi, M. Investigation of annealing treatment on the interfacial properties of explosive-welded Al/Cu/Al multilayer. *Mater. Des.* **2012**, *37*, 122–127, doi:10.1016/j.matdes.2011.12.045.
46. Sedighi, M.; Honarpisheh, M. Experimental study of through-depth residual stress in explosive welded Al–Cu–Al multilayer. *Mater. Des.* **2012**, *37*, 577–581, doi:10.1016/j.matdes.2011.10.022.
47. Asemabadi, M.; Sedighi, M.; Honarpisheh, M. Investigation of cold rolling influence on the mechanical properties of explosive-welded Al/Cu bimetal. *Mater. Sci. Eng. A* **2012**, *558*, 144–149, doi:10.1016/j.msea.2012.07.102.
48. Gong, S.; Li, Z.; Xiao, Z.; Zheng, F. Microstructure and property of the composite laminate cladded by explosive welding of CuAlMn shape memory alloy and QBe2 alloy. *Mater. Des.* **2009**, *30*, 1404–1408, doi:10.1016/j.matdes.2008.06.067.
49. Kaçar, R.; Acarer, M. Microstructure–property relationship in explosively welded duplex stainless steel–steel. *Mater. Sci. Eng. A* **2003**, *363*, 290–296, doi:10.1016/S0921-5093(03)00643-9.
50. Liu, L.; Jia, Y.-F.; Xuan, F.-Z. Gradient effect in the waved interfacial layer of 304L/533B bimetallic plates induced by explosive welding. *Mater. Sci. Eng. A* **2017**, *704*, 493–502, doi:10.1016/j.msea.2017.08.012.
51. Rajani, H.R.Z.; Mousavi, S.A.A.A.; Madani Sani, F. Comparison of corrosion behavior between fusion cladded and explosive cladded Inconel 625/plain carbon steel bimetal plates. *Mater. Des.* **2013**, *43*, 467–474, doi:10.1016/j.matdes.2012.06.053.
52. Rajani, H.R.Z.; Mousavi, S.A.A.A. The effect of explosive welding parameters on metallurgical and mechanical interfacial features of Inconel 625/plain carbon steel bimetal plate. *Mater. Sci. Eng. A* **2012**, *556*, 454–464, doi:10.1016/j.msea.2012.07.012.
53. Rajani, H.R.Z.; Mousavi, S.A.A.A. The Role of Impact Energy in Failure of Explosive Cladding of Inconel 625 and Steel. *J. Fail. Anal. Prev.* **2012**, *12*, 646–653, doi:10.1007/s11668-012-9601-1.
54. Lazurenko, D.V.; Bataev, I.A.; Mali, V.I.; Lozhkina, E.A.; Esikov, M.A.; Bataev, V.A. Structural Transformations Occurring upon Explosive Welding of Alloy Steel and High-Strength Titanium. *Phys. Met. Metallogr.* **2018**, *119*, 469–476, doi:10.1134/S0031918X18050095.
55. Lazurenko, D.V.; Bataev, I.A.; Mali, V.I.; Esikov, M.A.; Bataev, A.A. Effect of Hardening Heat Treatment on the Structure and Properties of a Three-Layer Composite of Type 'VT23-08ps-45KhNM' Obtained by Explosion Welding. *Met. Sci. Heat Treat.* **2019**, *60*, 651–658, doi:10.1007/s11041-019-00333-1.
56. Chen, P.; Feng, J.; Zhou, Q.; An, E.; Li, J.; Yuan, Y.; Ou, S. Investigation on the Explosive Welding of 1100 Aluminum Alloy and AZ31 Magnesium Alloy. *J. Mater. Eng. Perform.* **2016**, *25*, 2635–2641, doi:10.1007/s11665-016-2088-2.
57. Feng, J.; Chen, P.; Zhou, Q. Investigation on Explosive Welding of Zr53Cu35Al12 Bulk Metallic Glass with Crystalline Copper. *J. Mater. Eng. Perform.* **2018**, *27*, 2932–2937, doi:10.1007/s11665-018-3396-5.
58. Bataev, I.A.; Bataev, A.A.; Mali, V.I.; Pavliukova, D.V. Structural and mechanical properties of metallic–intermetallic laminate composites produced by explosive welding and annealing. *Mater. Des.* **2012**, *35*, 225–234, doi:10.1016/j.matdes.2011.09.030.
59. Lazurenko, D.V.; Bataev, I.A.; Mali, V.I.; Bataev, A.A.; Maliutina, I.N.; Lozhkin, V.S.; Esikov, M.A.; Jorge, A.M.J. Explosively welded multilayer Ti-Al composites: Structure and transformation during heat treatment. *Mater. Des.* **2016**, *102*, 122–130, doi:10.1016/j.matdes.2016.04.037.
60. Hokamoto, K.; Chiba, A.; Fujita, M.; Izuma, T. Single-shot explosive welding technique for the fabrication of multilayered metal base composites: Effect of welding parameters leading to optimum bonding condition. *Compos. Eng.* **1995**, *5*, 1069–1079, doi:10.1016/0961-9526(95)00059-V.
61. Chu, Q.L.; Zhang, M.; hong Li, J.; Jin, Q.; yang Fan, Q.; wei Xie, W.; Luo, H.; yue Bi, Z. Experimental investigation of explosion-welded CP-Ti/Q345 bimetallic sheet filled with Cu/V based flux-cored wire. *Mater. Des.* **2015**, *67*, 606–614, doi:10.1016/j.matdes.2014.11.008.

62. Wang, P.; Chen, J.; Li, Q.; Liu, D.; Huang, P.; Jin, F.; Zhou, Y.; Yang, B. Study on the microstructure and properties evolution of CuCrZr/316LN-IG explosion bonding for ITER first wall components. *Fusion Eng. Des.* **2017**, *124*, 1135–1139, doi:10.1016/j.fusengdes.2017.02.030.
63. Wang, Y.; Li, X.; Wang, X.; Yan, H. Fabrication of a thick copper-stainless steel clad plate for nuclear fusion equipment by explosive welding. *Fusion Eng. Des.* **2018**, *137*, 91–96, doi:10.1016/j.fusengdes.2018.08.017.
64. Yang, M.; Ma, H.; Shen, Z.; Sun, Y. Study on explosive welding for manufacturing meshing bonding interface of CuCrZr to 316L stainless steel. *Fusion Eng. Des.* **2019**, *143*, 106–114, doi:10.1016/j.fusengdes.2019.03.137.
65. Wang, T.; Zhang, F.; Li, X.; Jiang, S.; Feng, J. Interfacial evolution of explosively welded titanium/steel joint under subsequent EBW process. *J. Mater. Process. Technol.* **2018**, *261*, 24–30, doi:10.1016/j.jmatprotec.2018.05.031.
66. Yang, M.; Ma, H.; Shen, Z.; Chen, D.; Deng, Y. Microstructure and mechanical properties of Al-Fe meshing bonding interfaces manufactured by explosive welding. *Trans. Nonferr. Met. Soc. China* **2019**, *29*, 680–691, doi:10.1016/S1003-6326(19)64978-2.
67. Bataev, I.A.; Lazurenko, D.V.; Tanaka, S.; Hokamoto, K.; Bataev, A.A.; Guo, Y.; Jorge, A.M. High cooling rates and metastable phases at the interfaces of explosively welded materials. *Acta Mater.* **2017**, *135*, 277–289, doi:10.1016/j.actamat.2017.06.038.
68. Andreevskikh, L.A.; Drozdov, A.A.; Mikhailov, A.L.; Samarokov, Y.M.; Skachkov, O.A.; Deribas, A.A. Producing bimetallic steel-copper composites by explosive welding. *Steel Transl.* **2015**, *45*, 84–87, doi:10.3103/S0967091215010027.
69. Blatter, A.; Peguiron, D.A. Explosive joining of precious metals. *Gold Bull.* **1998**, *31*, 93–98, doi:10.1007/BF03214769.
70. Chu, Q.; Tong, X.; Xu, S.; Zhang, M.; Li, J.; Yan, F.; Yan, C. Interfacial Investigation of Explosion-Welded Titanium/Steel Bimetallic Plates. *J. Mater. Eng. Perform.* **2020**, *29*, 78–86, doi:10.1007/s11665-019-04535-9.
71. Greenberg, B.A.; Ivanov, M.A.; Inozemtsev, A.V.; Pushkin, M.S.; Patselov, A.M.; Besshaposhnikov, Y.R. Comparative characterisation of interfaces for two- and multi-layered Cu-Ta explosively welded composites. *Compos. Interfaces* **2020**, *27*, 705–715, doi:10.1080/09276440.2019.1690352.
72. Sun, Z.; Shi, C.; Wu, X.; Shi, H. Comprehensive investigation of effect of the charge thickness and stand-off gap on interface characteristics of explosively welded TA2 and Q235B. *Compos. Interfaces* **2020**, 1–17, doi:10.1080/09276440.2020.1716578.
73. Guo, X.; Ma, Y.; Jin, K.; Wang, H.; Tao, J.; Fan, M. Effect of Stand-Off Distance on the Microstructure and Mechanical Properties of Ni/Al/Ni Laminates Prepared by Explosive Bonding. *J. Mater. Eng. Perform.* **2017**, *26*, 4235–4244, doi:10.1007/s11665-017-2890-5.
74. Zhou, Q.; Feng, J.; Chen, P. Numerical and Experimental Studies on the Explosive Welding of Tungsten Foil to Copper. *Materials* **2017**, *10*, 984, doi:10.3390/ma10090984.
75. Tao, C.; Li, J.; Lu, M.; Yang, X.; Zhao, H.; Wang, W.; Zhu, W. Microstructure and mechanical properties of Cu/CuCrZr composite plates fabricated by explosive welding. *Compos. Interfaces* **2020**, 1–12, doi:10.1080/09276440.2020.1722519.
76. Sahul, M.; Sahul, M.; Lokaj, J.; Čaplovič, L.; Nesvadba, P. Influence of Annealing on the Properties of Explosively Welded Titanium Grade 1—AW7075 Aluminum Alloy Bimetals. *J. Mater. Eng. Perform.* **2018**, *27*, 5665–5674, doi:10.1007/s11665-018-3667-1.
77. Sahul, M.; Sahul, M.; Lokaj, J.; Čaplovič, Ľ.; Nesvadba, P.; Odokienová, B. The Effect of Annealing on the Properties of AW5754 Aluminum Alloy-AZ31B Magnesium Alloy Explosively Welded Bimetals. *J. Mater. Eng. Perform.* **2019**, *28*, 6192–6208, doi:10.1007/s11665-019-04361-z.
78. Saravanan, S.; Raghukandan, K.; Kumar, P. Effect of wire mesh interlayer in explosive cladding of dissimilar grade aluminum plates. *J. Cent. South Univ.* **2019**, *26*, 604–611, doi:10.1007/s11771-019-4031-9.
79. Yazdani, M.; Toroghinejad, M.R.; Hashemi, S.M. Investigation of Microstructure and Mechanical Properties of St37 Steel-Ck60 Steel Joints by Explosive Cladding. *J. Mater. Eng. Perform.* **2015**, *24*, 4032–4043, doi:10.1007/s11665-015-1670-3.
80. Fang, Z.; Shi, C.; Shi, H.; Sun, Z. Influence of Explosive Ratio on Morphological and Structural Properties of Ti/Al Clads. *Metals* **2019**, *9*, 119, doi:10.3390/met9020119.
81. Mahmood, Y.; Dai, K.; Chen, P.; Zhou, Q.; Bhatti, A.A.; Arab, A. Experimental and Numerical Study on Microstructure and Mechanical Properties of Ti-6Al-4V/Al-1060 Explosive Welding. *Metals* **2019**, *9*, 1189, doi:10.3390/met9111189.

82. Cui, Y.; Liu, D.; Zhang, Y.; Deng, G.; Fan, M.; Chen, D.; Sun, L.; Zhang, Z. The Microstructure and Mechanical Properties of TA1-Low Alloy Steel Composite Plate Manufactured by Explosive Welding. *Metals* **2020**, *10*, 663, doi:10.3390/met10050663.